Cosmic Masers - from OH to H_0
Proceedings IAU Symposium No. 287, 2012
R.S. Booth, E.M.L. Humphreys & W.H.T. Vlemmings, eds.

doi:10.1017/S1743921312007363

VLBI maser kinematics in high-mass SFRs: G23.01–0.41

Alberto Sanna[1], Luca Moscadelli[2], Riccardo Cesaroni[2] and Ciriaco Goddi[3]

[1]Max-Planck-Institut für Radioastronomie, Auf dem Hügel 69, 53121 Bonn, Germany
email: asanna@mpifr-bonn.mpg.de

[2]INAF, Osservatorio Astrofisico di Arcetri, Largo E. Fermi 5, 50125 Firenze, Italy
email: mosca@arcetri.astro.it; cesa@arcetri.astro.it

[3]European Southern Observatory, Karl-Schwarzschild-Strasse 2, D-85748 Garching bei München, Germany
email: cgoddi@eso.org

Abstract. Very Long Baseline Interferometry studies of different maser species observed at multiple epochs allow complementary measurements of the 3-dimensional velocity field of gas close ($\lesssim 10^3$AU) to massive young stellar objects. Here, we review our recent results toward the high-mass star-forming region G23.01–0.41, where all the strongest molecular maser transitions known to date cluster within 2000 AU from the center of an hot molecular core and are associated with a so called extended green object. The overall maser kinematics reveals a common outflowing motion from a central object; the details of the spatial distribution and velocity field of each maser species hint at the presence of different dynamical structures: a collimated jet, a wide-angle wind, and a flattened rotating core. We further compare the simultaneous presence of maser emission from different molecular species with a recent evolutionary sequence for masers associated with massive young stellar objects.

Keywords. masers, techniques: high angular resolution, stars: formation, stars: individual (G23.01–0.41).

1. Introduction

How do high-mass stars ($M_{star} > 8$ $M_\odot$) form? And what are the physical properties and dynamics of their environments locally? Maser emission in high-mass star-forming regions (HMSFRs) is a signpost of the earliest evolutionary phases of massive young stellar objects (MYSOs). The spatial compactness and the narrow linewidth (owing to the required high degree of velocity coherence) make maser emission an ideal tool for testing ordered velocity fields from the inner protostellar cocoon ($\lesssim 10^3$AU). At typical distances of a few kpc for MYSOs, mas-resolution (i.e., Very Long Baseline Interferometry, VLBI) observations of the spatial distribution of each masing cloudlets (as small as a few AU) monitored over time allows us to measure the full-space kinematics of the masing gas. In particular, those sites exhibiting multiple molecular masers gain greater interest since different molecular species can trace distinct and complementary physical environments, thus providing us with information useful to distinguish among different dynamical processes such as rotation, expansion, or contraction.

Almost a decade ago, we started a campaign of multi-epoch, VLBI observations of the three most powerful maser transitions, of water (H_2O) at 22.2 GHz, methanol (CH_3OH) at 6.7 GHz, and hydroxyl (OH) at 1.665 GHz toward HMSFRs already well studied with interferometers in thermal, continuum and line emission (e.g., Moscadelli *et al.* 2007,2011; Goddi *et al.* 2007,2011; Sanna *et al.* 2010a,b). Our idea was to complement

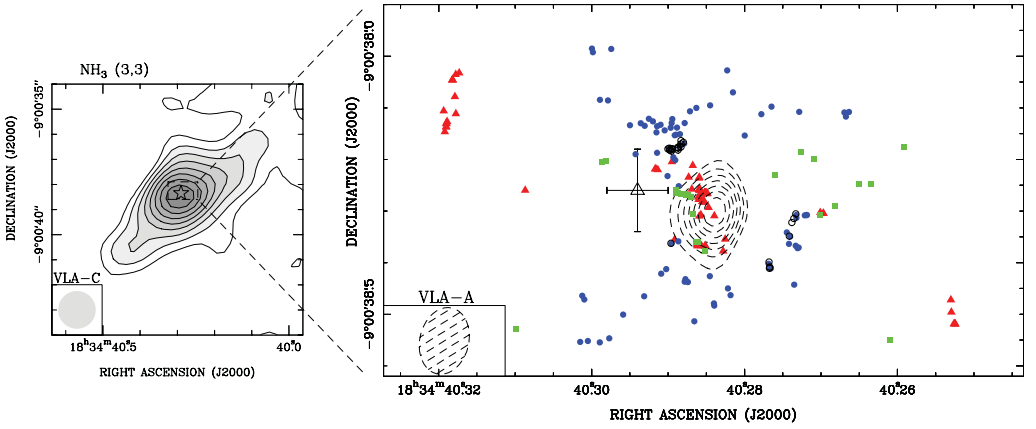

Figure 1. Collection of the subarcsec observations toward G23.01–0.41. *Left panel:* map of the NH_3 (3,3) line from Codella *et al.* (1997) with contour levels at multiples of 10% of the peak emission (46 mJy beam^{-1}). The star marks the peak position of the 3 mm continuum emission as determined by Furuya *et al.* (2008). *Right panel:* zoom in on the maser emitting region. Red triangles, blue dots, and green squares represent respectively H_2O, CH_3OH, and OH maser positions from our VLBI measurements (Sanna *et al.* 2010b). The empty circles mark the position of the 12.2 GHz CH_3OH maser cloudlets (Sanna *et al.* in prep.). The empty triangle with the error bars indicates the position (and the associated uncertainty) of the 4.8 GHz H_2CO maser feature derived by Araya *et al.* (2008). Dashed contours show the 1.3 cm continuum emission with contour levels at multiples of 10% of the peak emission (0.72 mJy beam^{-1}).

the information from thermal tracers of outflows (e.g., CO and SiO) and hot molecular cores (HMCs) e.g., dust continuum, NH_3, and CH_3CN), at typical scales from about 0.1 pc to several 1000 AU, with that on the inner few 1000 AU from the (proto)star, provided by maser emission and radio continuum from shock-induced ionization (i.e., thermal jets/winds) or photoionization by the central MYSO (i.e., young H II regions).

2. An overview of G23.01–0.41

G23.01–0.41 is an active site of massive star formation ($L_{bol} \sim 10^5 L_\odot$) with a copious amount of maser emission from different molecular species (see Tab. 1). This star-forming region has an accurate distance measurement of 4.6 ± 0.4 kpc, determined through the trigonometric parallax of the associated 12 GHz methanol masers (Brunthaler *et al.* 2009; see also the chapter by Reid *et al.*), and belongs to a larger star-forming complex possibly triggered by the close supernova remnant W41 (Leahy & Tian 2008). On a pc scale, the 4.5 μm excess of the Spitzer IRAC GLIMPSE observations (Benjamin *et al.* 2003; see also Cyganowski *et al.* 2009, their Figure 1) show a shocked molecular clump powered by a massive, ^{12}CO bipolar outflow detected with the IRAM interferometer by Furuya *et al.* (2008). Because of the small width-to-length ratio of both the blueshifted and redshifted outflow lobes (to the NE and SW, respectively), such a geometry indicates that the inclination angle of the outflow axis with respect to the plane of the sky must be rather small (particularly evident in our new SMA observations; Sanna *et al.* in prep.). Following the statistical analysis by Cyganowski *et al.* (these proceedings), the association of G23.01–0.41 with such an extended green object (EGO) suggests an enhanced outflow activity at an early stage of massive star formation, and thus (presumably) an actively accreting MYSO. At ten-times smaller scale, CH_3CN and NH_3 thermal emissions reveal an HMC of 70 $M_\odot$ with a flattened structure and a velocity gradient (~ 1 km s^{-1} over 0.1 pc) along its major axis (Furuya et al. 2008; Codella *et al.* 1997). Since the HMC is

https://doi.org/10.1017/S1743921312007363 Published online by Cambridge University Press

Table 1. Overall maser detections/upper limits toward G23.01–0.41

Molecule	ν (GHz)	Telescope	F_{peak} (Jy)	V_{LSR} (km s^{-1})	Ref.[1]
H_2O	22.2	VLBA	320	72.6	1
OH	1.612	Nançay Radio tel.	0.2	78	2
	1.665	VLBA	2.6	67.9	1
	1.667	Nançay Radio tel.	9	75	2
CH_3OH	6.7	EVN	440	74.7	1
	12.2	VLBA	20	75.0	3
	19.9	Tidbinbilla 70-m	< 0.26		4
	23.1	Parkes 64-m	< 0.9		5
	37.7	Mopra 22-m	< 0.9		6
	38.3	Mopra 22-m	< 0.9		6
	38.5	Mopra 22-m	< 0.9		6
	44.1	Parkes 64-m	40	77.1	7
	85.5	SEST	< 3.8		8
	95.2	Mopra 22-m	3	77.4	9
	107.0	SEST	5.2	75.9	10
	108.8	Mopra 22-m	< 5.1		11
	156.6	SEST	< 2		10
H_2CO	4.8	VLA-B	0.048	73.6	12

Notes:
F_{peak} and V_{LSR} are the peak flux density and its Local Standard of Rest velocity for each maser transition, respectively.
[1] Ref.: (1) Sanna *et al.* (2010b); (2) Szymczak & Gérard (2004); (3) Brunthaler *et al.* (2009); (4) Ellingsen *et al.* (2004); (5) Cragg *et al.* (2004); (6) Ellingsen *et al.* (2011); (7) Slysh *et al.* (1994); (8) Cragg *et al.* (2001); (9) Val'tts *et al.* (2000); (10) Caswell *et al.* (2000); (11) Val'tts *et al.* (1999); (12) Araya *et al.* (2008).

close to the center of the bipolar outflow and is elongated perpendicular to the outflow axis, it has been interpreted as a candidate rotating toroid, i.e. a massive, non-equilibrium structure accreting onto the embedded (proto)star(s) over a timescale shorter than its rotation period.

All the strongest maser species known to date are observed to cluster at the center of the HMC together with faint continuum emission at centimeter wavelengths (Sanna *et al.* 2010b; Brunthaler *et al.* 2009; Araya *et al.* 2008). The spectral index of the radio continuum is consistent with shock excited emission from a thermal jet, whereas its spatial morphology at the longest VLA baselines clearly draws a bright knot along the NE–SW direction of the molecular outflow (Sanna *et al.* 2010b). Between 2005 and 2007, we conducted phase-referencing, VLBA and EVN observations of the H_2O, CH_3OH (both at several epochs), and of the OH masers (at a single epoch) in the K, C, and L bands, respectively (see Tab. 1). Recently, we have also complemented this data set with archival VLBA observations in the U band, in order to study the details of the methanol maser kinematics at 12 GHz with respect to the 6.7 GHz transition (Sanna *et al.* in prep.). These observations reveal that all the maser emissions in the region participate in an overall expansion from a common center, which possibly denotes the position of the YSO (Sanna *et al.* 2010b). Furthermore, these maser species sample different positions in the gas around G23.01–0.41 and their radial and transverse velocities pinpoint 3 distinct kinematical structures (see Fig. 1). The H_2O masers trace both: I) shocked gas along the route of the same bipolar jet exciting the radio continuum and II) a wide-angle, faster wind projected close to the putative position of the YSO (where H_2O masers are also flaring; see Figure 5b of Sanna *et al.* 2010b). Similarly, the OH masers projected close to the fast-moving water masers are strongly blueshifted with respect to the systemic velocity of the region (Figure 3c of Sanna *et al.* 2010b). We have hypothesized that: I) this emission may be tracing an expanding layer of gas at a larger distance from the YSO

https://doi.org/10.1017/S1743921312007363 Published online by Cambridge University Press

than the H_2O gas and II) the same wide-angle wind responsible for the fast water maser shocks could power the expansion of the OH gas. Finally, the spatial distribution and velocity field of the CH_3OH cloudlets sketch out a funnel-like structure that probably results from a combination of both rotation and expansion inside the NH_3 toroid (Figure 6 of Sanna *et al.* 2010b).

3. Details on the Maser Emission

Water masers. It is interesting to note that, the momentum rate of the water maser jet can be directly compared with that of the large-scale ^{12}CO outflow. This calculation shows consistent values of a few 0.1 $M_\odot$ yr^{-1} km s^{-1} and has two implications: I) it brings further support to the hypothesis that water masers more detached from the radio continuum trace the primary wind (i.e., the jet) driving the large-scale molecular outflow; II) provided that molecular outflows are momentum driven and their momentum rate is correlated with the mass and luminosity of the YSO (e.g., Figure 4 of Beuther *et al.* 2002), the high value measured above implies indeed a ZAMS star of early B/late O spectral type. Furthermore, the detection of a wide-angle wind from water masers close to the MYSO can explain the observation of a width-to-length ratio for the molecular outflow of $\sim 0.4 - 0.3$, much higher than in a pure jet-driven outflow.

Methanol masers. Focusing on the 6.7 GHz maser transition, by observing 3 different EVN epochs spanning 2 years, *we have measured for the first time the internal proper motions of individual, methanol maser cloudlets with relative uncertainties less than 30%* (together with the source G16.59–0.05 from Sanna *et al.* 2010a). The line-of-sight velocity distribution is clearly bipolar, showing two distinct groups of methanol masers, one moving away from the observer (southern redshifted cluster) and one toward the observer (northern blueshifted cluster). By studying the distribution of the 3-dimensional methanol maser velocities with respect to the jet direction on the sky and its inclination with respect to the l.o.s., we have proposed that the methanol gas undergoes rotation about the jet axis and is simultaneously dragged into the outflow motion along this axis (Figure 8 of Sanna *et al.* 2010b). If we assume centrifugal equilibrium, the rotational component inferred from the velocity field of the methanol gas implies again a central, massive ZAMS star with an early B/late O spectral type. A further, detailed comparison of the spatial distribution and kinematics of the strong maser emission at 12 GHz and 6.7 GHz suggests that both transitions are excited from the same methanol gas (Sanna *et al.* in prep.). According to Cragg *et al.* (2005), this evidence constrains the gas temperature and density to values of T_k = 30–50 K and $n_{H_2} = 10^6$–10^7 cm^{-3}, well in agreement with the physical parameters of the ammonia core. This analysis strongly supports the hypothesis that the Class II CH_3OH masers may emerge from the inner part of the massive toroid traced on a larger scale with the CH_3CN and NH_3 molecules. It is also worth noting that G23.01–0.41 is one of the rare cases where H_2CO maser emission at 4.8 GHz was recently found by Araya *et al.* (2008). This emission arising from a region consistent both in position and l.o.s. velocity with the blueshifted methanol masers may, when refined models for H_2CO pumping mechanism become available (e.g., Araya *et al.* 2007), help to further constrain the physical conditions in the region.

Evolutionary sequence in G23.01–0.41. Finally, we want to use a recent evolutionary sequence proposed to explain the appearance and relative lifetimes of different maser species in HMSFRs (cf. Figure 6 of Breen *et al.* 2010; see also Breen *et al.*, these proceedings) to speculate on the relative phase of evolution for G23.01–0.41. First of all, the star-forming region is associated with strong 4.5 μm emission (i.e., an EGO) and shows also bright 44 GHz methanol masers along the direction of the outflow (e.g., Cyganowski

https://doi.org/10.1017/S1743921312007363 Published online by Cambridge University Press

et al. 2009). The presence of Class I methanol masers and strong outflow activity, together with our findings of faint radio continuum emission mostly due to shock-induced ionization, rule out the far side of the Breen's scale, where photoionization from the central MYSO should produce a bright UCH II region. On the other hand, very bright 6.7 GHz and 12 GHz methanol masers (as found in G23.01–0.41) seem to be associated with a somewhat late stage of evolution for MYSO (Breen *et al.* 2011), that rules out the first half of the Breen's scale as well. The evidence for an intermediate evolutionary phase of G23.01–0.41 is further supported by the simultaneous presence of bright, main-line, OH masers, that are usually found in the vicinity of a detectable UCH II region. Following this evolutionary sequence, we can speculate that: I) G23.01–0.41 should develop in the near future a visible UCH II region; II) since high accretion rates are the main mechanism proposed for quenching of UCH II regions, G23.01–0.41 should be still actively accreting material from its protostellar envelope, that would be detectable with ALMA observations of thermal, dense gas tracers.

Acknowledgements

This work has been supported by the ERC Advanced Grant GLOSTAR under grant agreement no. 247078.

References

Araya, E., Hofner, P., & Goss, W. M. 2007, IAU Symposium, 242, 110
Araya, E. D., Hofner, P., Goss, W. M., *et al.* 2008, *ApJS*, 178, 330
Benjamin, R. A., Churchwell, E., Babler, B. L., *et al.* 2003, *PASP*, 115, 953
Beuther, H., Schilke, P., Sridharan, T. K., *et al.* 2002, *A&A*, 383, 892
Breen, S. L., Ellingsen, S. P., Caswell, J. L., & Lewis, B. E. 2010, *MNRAS*, 401, 2219
Breen, S. L., Ellingsen, S. P., Caswell, J. L., *et al.* 2011, *ApJ*, 733, 80
Brunthaler, A., Reid, M. J., Menten, K. M., *et al.* 2009, *ApJ*, 693, 424
Caswell, J. L., Yi, J., Booth, R. S., & Cragg, D. M. 2000, *MNRAS*, 313, 599
Codella, C., Testi, L., & Cesaroni, R. 1997, *A&A*, 325, 282
Cragg, D. M., Sobolev, A. M., Ellingsen, S. P., *et al.* 2001, *MNRAS*, 323, 939
Cragg, D. M., Sobolev, A. M., Caswell, J. L., Ellingsen, S. P., & Godfrey, P. D. 2004, *MNRAS*, 351, 1327
Cragg, D. M., Sobolev, A. M., & Godfrey, P. D. 2005, *MNRAS*, 360, 533
Cyganowski, C. J., Brogan, C. L., Hunter, T. R., & Churchwell, E. 2009, *ApJ*, 702, 1615
Ellingsen, S. P., Cragg, D. M., Lovell, J. E. J., *et al.* 2004, *MNRAS*, 354, 401
Ellingsen, S. P., Breen, S. L., Sobolev, A. M., *et al.* 2011, *ApJ*, 742, 109
Furuya, R. S., Cesaroni, R., Takahashi, S., *et al.* 2008, *ApJ*, 673, 363
Goddi, C., Moscadelli, L., Sanna, A., Cesaroni, R., & Minier, V. 2007, *A&A*, 461, 1027
Goddi, C., Moscadelli, L., & Sanna, A. 2011, *A&A*, 535, L8
Leahy, D. A. & Tian, W. W. 2008, *AJ*, 135, 167
Moscadelli, L., Goddi, C., Cesaroni, R., Beltrán, M. T., & Furuya, R. S. 2007, *A&A*, 472, 867
Moscadelli, L., Cesaroni, R., Rioja, M. J., Dodson, R., & Reid, M. J. 2011, *A&A*, 526, A66
Sanna, A., Moscadelli, L., Cesaroni, R., *et al.* 2010a, *A&A*, 517, A71
Sanna, A., Moscadelli, L., Cesaroni, R., *et al.* 2010b, *A&A*, 517, A78
Slysh, V. I., Kalenskii, S. V., Valtts, I. E., & Otrupcek, R. 1994, *MNRAS*, 268, 464
Szymczak, M. & Gérard, E. 2004, *A&A*, 414, 235
Val'tts, I. E., Ellingsen, S. P., Slysh, V. I., *et al.* 1999, *MNRAS*, 310, 1077
Val'tts, I. E., Ellingsen, S. P., Slysh, V. I., *et al.* 2000, *MNRAS*, 317, 315